

# Rayleigh–Taylor instability of ionization front around black holes

KwangHo Park<sup>1\*</sup>, Massimo Ricotti<sup>2,3</sup>, Tiziana Di Matteo<sup>1</sup>, and Christopher S. Reynolds<sup>2</sup>

<sup>1</sup>*McWilliams Center, Carnegie Mellon University, Pittsburgh, PA 15213, USA*

<sup>2</sup>*Department of Astronomy, University of Maryland, College Park, MD 20740, USA*

<sup>3</sup>*Sorbonne Universités, Institut Lagrange de Paris (ILP), 98 bis Boulevard Arago 75014 Paris, France*

Accepted 2013 October 28. Received 2013 October 17; in original form 2013 August 22

## ABSTRACT

We examine the role of ionizing radiation emitted from black holes (BHs) in suppressing the growth of the Rayleigh–Taylor instability (RTI) across the ionization front (I-front) that forms when the gas fuelling the BH is neutral. We use radiation-hydrodynamic simulations to show that the RTI is suppressed for non-accelerating fronts on all scales resolved in our simulations. A necessary condition for the stability of the I-front is that the radius of the Strömgen sphere is larger than the Bondi radius. When this condition is violated the I-front collapses producing an accretion luminosity burst. Transient growth of the RTI occurs only during the accretion burst when the effective acceleration in the frame of reference of the I-front increases significantly due to the rapid expansion of the Strömgen sphere.

**Key words:** accretion, accretion discs – black hole physics – hydrodynamics – instabilities – radiative transfer methods: numerical.

## 1 INTRODUCTION

Rayleigh–Taylor instability (RTI) develops across an interface between two media with different densities with a presence of background gravitational acceleration or when the density front is accelerating (Taylor 1950; Chandrasekhar 1961). Gravity accelerates high-density gas into the low-density medium, leading to an exponential growth of the instability. In astrophysical circumstances, special attention has been paid to the RTI coupled with radiation field in star-forming H II regions or black hole (BH) systems (Kahn 1958; Krolik 1977; Krumholz & Matzner 2009; Jacquet & Krumholz 2011; Kuiper et al. 2012; Jiang, Davis, & Stone 2013). In particular, Mizuta et al. (2005) studied the growth of RTI at the ionization fronts (I-fronts) produced by UV photons from massive star formation and showed that recombination in the ionized gas suppresses the growth of RTI.

Similarly, ionizing UV and X-ray photons emitted by BHs embedded in a neutral medium produce a *D*-type (dense) I-front that should be unstable to RTI. The hydrogen ionizing photons heat the surrounding gas that expands producing a hot, rarefied and ionized medium opposing the collapse of the denser ambient medium subject to the BH gravitational field. The RTI can act as an effective mechanism for delivering high-density gas to the central gravitating source (e.g., Krumholz et al. 2009). Thus, understanding of the RTI around luminous gravitational sources such as proto-stellar cores or BHs, is of critical importance for estimating their accretion rates, which might enhance the final mass of stellar cores or the growth rate of BHs. In particular, the accretion rate on to a BH

is directly related to the energy it emits but the enhanced luminosity may also suppress the gas supply to the BH. Therefore, the onset of RTI could be important for the mechanism of self-regulation of BH growth.

In this paper, we perform radiation-hydrodynamic simulations to examine the special case of RTI in the context of radiation-regulated accretion on to BHs. The main goal of this study is to test whether the RTI plays an important role in supplying high-density gas to the central BHs and to identify the physical conditions for the stability of the I-front. In Section 2, we discuss the phenomenology related to RTI found in our previous studies while we explain the relevant physical scales and the numerical simulations in Section 3. In Section 4, we show the numerical results, and finally, we summarize and discuss the results in Section 5.

## 2 MOTIVATION

UV and X-ray photons emitted from a BH accreting from a neutral medium, create a hot and ionized bubble of gas (i.e., a Strömgen sphere) around the BH. A *D*-type I-front separates the ionized gas from the neutral higher density gas. In Park & Ricotti (2011, 2012, 2013), we explored the role of the Strömgen sphere in regulating the gas supply from large scales to the BH. We found a periodic variation of accretion luminosity and thus the size of the Strömgen sphere (Milosavljević, Couch, & Bromm 2009; Li 2011) determined by the thermal structure of the gas inside the Strömgen sphere. Park & Ricotti (2012) found that the average accretion rate is typically 1 per cent of the Bondi accretion rate of the neutral gas when it is radiation-regulated. In this regime, the average accretion rate is comparable to the Bondi rate in the ion-

\* E-mail: kwanghop@andrew.cmu.edu

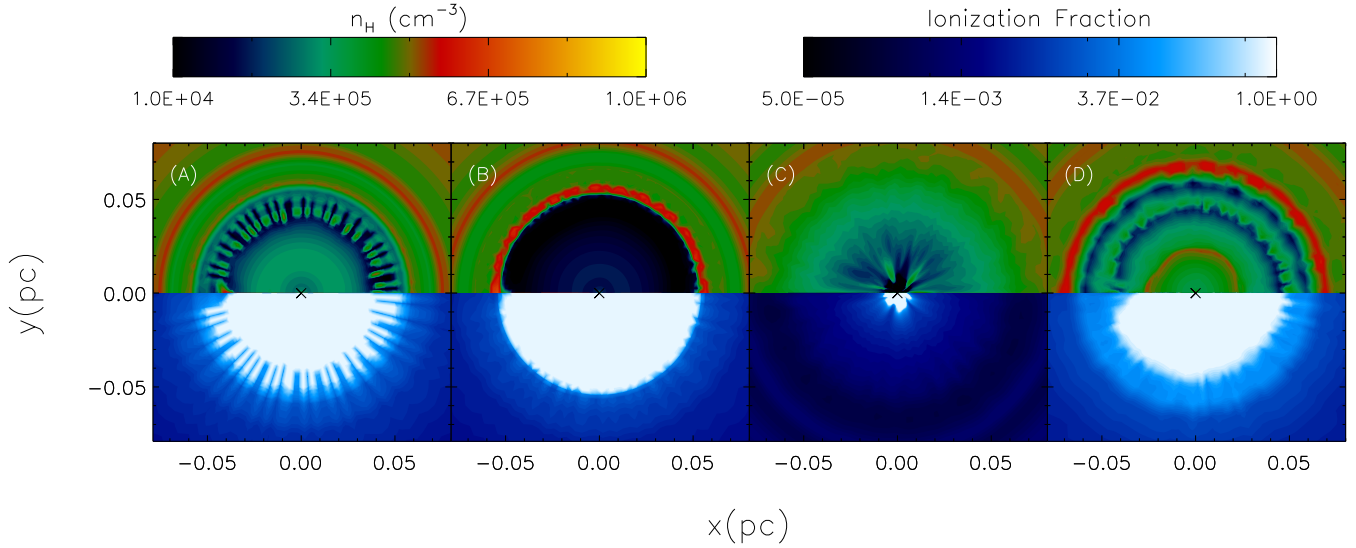


**Figure 1.** Snapshots from our previous 2D radiation-hydrodynamic simulation of radiation-regulated accretion on to a BH (Park & Ricotti 2011) of mass  $M_{\text{bh}} = 100 M_{\odot}$  surrounded by gas with density  $n_{\text{H},\infty} = 10^5 \text{ cm}^{-3}$ , and temperature  $T_{\infty} = 10^4 \text{ K}$ . RTI at the I-front develops transiently (A, C and D) when the BH luminosity increases mildly (A) or bursts (D), or at the collapsing moment of the I-front (C). However, the RTI observed throughout the simulations in various phase of the oscillation becomes suppressed as shown in (B) maintaining the spherical symmetry of the ionized H II region. The overall underlying hydrodynamic structure of the Strömgren sphere is ideal for the growth of the RTI since a low-density gas is surrounded by a high-density gas with an acceleration due to gravity; however, the radiation from the BHs suppresses the growth of the RTI. The condition for the transitory growth of the RTI matches well with the Equation (5) implying that RTI can grow temporarily when the density contrast between two media increases or the effective acceleration on the I-front increases (i.e. when the I-front expands outwards against the gravitational acceleration as shown in A and D).

ized gas that is lower than the Eddington limit when  $n_{\text{H},\infty} M_{\text{bh}} < 4 \times 10^8 \text{ cm}^{-3} M_{\odot}$ . In general, the effect of photon momentum is found to be negligible since the accretion rate shows oscillatory behaviour due to self-regulation. The acceleration due to radiation pressure is negligible compared to the gravity by the BH in the entire range of radius for most time of the quasi-periodic oscillation. However, for the case of momentum-driven I-front in the Eddington-limited regime, the photon momentum can be effective in enhancing the RTI across the I-front since radiation pressure increases the effective gravity at the I-front.

The Strömgren sphere should be subject to RTI since lower density (i.e., hot and ionized bubble) gas supports higher density neutral gas against the BH’s gravity. Moreover, the feedback loop generates sharp bursts of the BH luminosity, that result in a rapid increase of the size of the Strömgren sphere. When the Strömgren sphere expands during the luminosity burst, the RTI can grow on a shorter time-scale since the effective acceleration in the frame of reference of the I-front increases. However, our previous simulations (Park & Ricotti 2011, 2012) show that the I-front is remarkably stable to RTI, even for perturbations with short wavelength that should grow on time-scales shorter than the period between luminosity bursts when the Strömgren sphere is stationary. In addition, 1D and 2D simulations produce the same results in terms of accretion rate and period of the luminosity cycle. We observe a transitory development of the RTI only during the periodic luminosity bursts, however the growth of RTI fingers is quickly suppressed and does not fuel the BH. Instead, we typically observe a well-defined spherically symmetric low-density sphere that varies in size as a function of time. Snapshots in Fig. 1 (see also Park & Ricotti 2011) shows the transient development and suppression of the RTI. Panel (A) shows the RTI fingers when the I-front expands as a result of an increase of the BH luminosity, while panel

(B) displays the suppression of the RTI at the I-front and the recovered spherical symmetry of the Strömgren sphere. Front instabilities are typically observed just before and after a luminosity burst. Panel (C) shows a snapshot at the time of collapse of the Strömgren sphere that leads to a luminosity burst. This happens when the BH luminosity reaches its minimum value in the cycle and the gas density inside the H II region has its lowest value. Panel (D) displays a snapshot at a time right after a luminosity burst, also showing instabilities.

In our previous simulations we focused on the mechanisms of self-regulation of gas accretion on to BHs. However, in those simulations it is difficult to examine the suppression mechanism of the RTI in detail because of the varying BH luminosity and size of the Strömgren sphere. In this paper, we focus on the growth/suppression of the RTI at I-front using controlled numerical experiments in which we keep the BH luminosity, the size of the Strömgren sphere, the amplitude and wavenumber of the perturbations fixed. We assume idealized spherically symmetric accretion on to stationary BHs from non-magnetized neutral gas with zero angular momentum. In particular, we investigate the RTI of I-front on the order of the Bondi radius scale where the gravity becomes dominant over the thermal energy of the neutral gas, and thus the RTI is effectively influenced. The present study, although idealized, illustrates the stabilizing effect of opacity to ionizing radiation to the development of RTI at I-fronts. The simplifying assumptions of spherical symmetry and small gas angular momentum are rather realistic at the scale of the Bondi radius in many astrophysical applications (galactic winds or active galactic nucleus winds); however, they are not critical to the development of the instability.

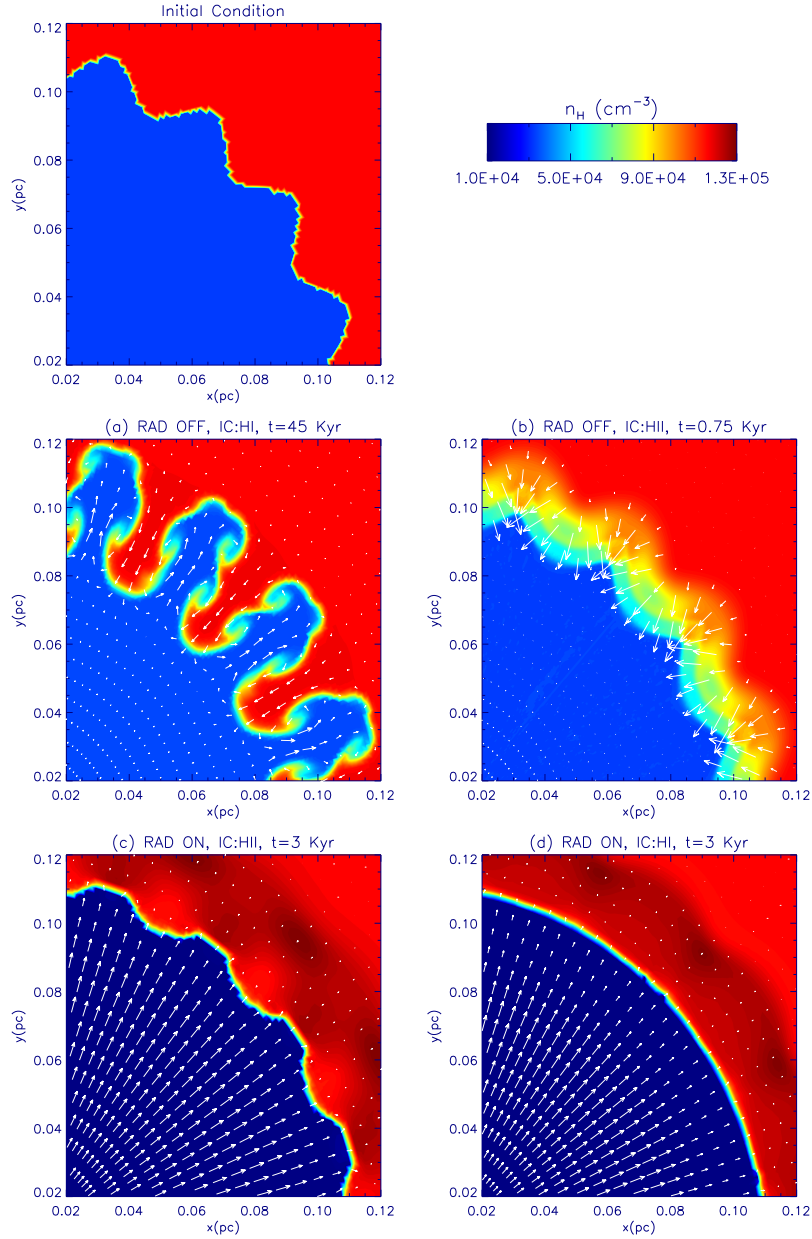


**Figure 2.** Growth and suppression of RTI in various condition for a BH of mass  $M_{\text{bh}} = 100 M_{\odot}$  surrounded by gas with a density  $n_{\text{H},\infty} = 10^5 \text{ cm}^{-3}$ . Initial temperature of the Strömgen sphere is set as  $T_{\text{in}} = 6 \times 10^4 \text{ K}$  and the density is set as  $n_{\text{H},\text{in}} = T_{\infty}/T_{\text{in}} n_{\text{H},\infty}$  so that the IC is in thermal equilibrium condition Top: density profile of the IC for all simulations (a)–(d). Panel (a): snapshot of the density profile taken at  $t = 45 \text{ Kyr}$  for the run K20RTI (no radiation from the BH). Panel (b): density snapshot taken at  $t = 0.75 \text{ Kyr}$  for the run K20RTIrec (low-density region is ionized at the IC and the radiation from the BH remains turned off during the simulation. Only the effect of recombination of ionized gas is considered in this simulation). Panel (c): density snapshot taken at  $t = 3 \text{ Kyr}$  for the run K20HII (radiation from the BH is on and the low-density region is ionized at the IC). Panel (d): density snapshot taken at  $t = 3 \text{ Kyr}$  for the run K20HI (radiation from the BH is on and the low-density region is neutral at the IC). Simulations become unstable to RTI when there is no radiation from the BH shown in (a) and (b) while the radiation from the BH suppresses the growth of RTI on the I-front effectively shown in (c) and (d). Photoionization and the thermal pressure gradient inside H II region effectively suppress the growth of the RTI. The recombination also dampens the initial perturbation effectively as shown in (b) and (d).

### 3 METHODOLOGY

In this section, we explain the basic equations and typical scales related to accretion physics, BH radiation, and RTI. We also describe the set-up of our numerical simulations.

#### 3.1 Strömgen Sphere in BH Systems

The Bondi equations describe spherically symmetric accretion on to a point source (Bondi & Hoyle 1944; Bondi 1952). The Bondi radius is the distance from the point source where the BH’s gravitational potential roughly equals the thermal energy of the surrounding gas. It is defined as  $r_{\text{B}} \equiv GM_{\text{bh}}/c_{\text{s},\infty}^2$ , where  $M_{\text{bh}}$  is the BH mass and  $c_{\text{s},\infty}$  is the sound speed of the neighbouring gas.

**Table 1.** Simulation parameters.

ID	$M_{\text{bh}}(M_{\odot})$	$\frac{L}{L_{\text{Edd}}}$	$n_{\text{H},\infty}(\text{cm}^{-3})$	$T_{\infty}(\text{K})$	$\frac{n_{\text{H},\infty}}{n_{\text{H},\text{in}}}$	$R_{\text{s},0}(\text{pc})$	$r_{\text{B}}$	$k$	IC	$\delta R_{\text{s},0}/R_{\text{s},0}$
K20RTI	$1 \times 10^2$	0.0	$10^5$	$10^4$	6.0	0.0	0.005	20	H I	0.05
K20RTIrec	$1 \times 10^2$	0.0	$10^5$	$10^4$	6.0	0.0	0.005	20	H II	0.05
K20HI	$1 \times 10^2$	$10^{-1}$	$10^5$	$10^4$	6.0	0.11	0.005	20	H I	0.05
K20, K40, K80	$1 \times 10^2$	$10^{-1}$	$10^5$	$10^4$	6.0	0.11	0.005	20, 40, 80	H II	0.05
RANE1–RANE5	$1 \times 10^2$	$10^{-1}$ – $10^{-5}$	$10^5$	$10^4$	6.0	0.11–0.005	0.005	496	H I	0.1, 0.2
T4A	$2 \times 10^5$	$5.0 \times 10^{-5}$	10	$10^4$	6.0	33	9	20	H II	0.1
T4B	$8 \times 10^5$	$1.25 \times 10^{-5}$	10	$10^4$	6.0	33	35	20	H II	0.1
T3A	$2 \times 10^5$	$5.0 \times 10^{-5}$	10	$10^3$	60.0	130	90	20	H II	0.1
T3B	$5 \times 10^5$	$2.0 \times 10^{-5}$	10	$10^3$	60.0	130	230	20	H II	0.1
T3ABURST	$2 \times 10^5$	$5.0 \times 10^{-5}$	10	$10^3$	60.0	130	90	12	H I	0.1

The Eddington luminosity  $L_{\text{Edd}}$  refers to the maximum luminosity that a BH can achieve assuming that the radiation pressure due to Compton scattering of photons on free electrons balances the BH's gravity:

$$L_{\text{Edd}} = \frac{4\pi GM_{\text{bh}}m_{\text{p}}c}{\sigma_{\text{T}}} \simeq 3.3 \times 10^4 M_{\text{bh},\odot} L_{\odot}. \quad (1)$$

Here,  $\sigma_{\text{T}}$  is the Thomson scattering cross-section and  $m_{\text{p}}$  is the proton mass. The dimensionless BH luminosity  $l$  is defined as  $l \equiv L/L_{\text{Edd}}$ . The number of ionizing photons  $N_{\text{ion}}$  emitted by the BH per unit time is

$$N_{\text{ion}} = \frac{L}{m \times 13.6 \text{ eV}} = 1.9 \times 10^{48} l M_{\text{bh},\odot} \text{ s}^{-1}, \quad (2)$$

where  $m = \alpha/(\alpha - 1)$  depends on the slope  $\alpha$  of the power-law spectrum of the BH radiation (we take  $\alpha = 1.5$  in this work). The size of the Strömgen sphere around the BH can be calculated from  $N_{\text{ion}}$  when the hydrogen number density,  $n_{\text{H}}$ , is known:  $N_{\text{ion}} = (4\pi/3)R_{\text{s}}^3 n_{\text{e}} n_{\text{H}} \alpha_{\text{rec}}$ , where we assume hydrogen recombination coefficient  $\alpha_{\text{rec}} = 4 \times 10^{-13} (T_{\text{in}}/10^4)^{-1/2} \text{ cm}^3 \text{ s}^{-1}$ . Therefore, the size of the Strömgen sphere is

$$R_{\text{s}} = 2.5 \times 10^{-3} \left( \frac{l M_{\text{bh},\odot}}{n_{\text{H}}^2 \alpha_{\text{rec}}} \right)^{1/3} \text{ pc}. \quad (3)$$

The assumption of thermal pressure equilibrium across the I-front is a good approximation only if  $R_{\text{s}} > r_{\text{B}}$ . Instead the I-front collapses on to the BH if  $R_{\text{s}} < r_{\text{B}}$ , or equivalently, when the thermal energy of the gas outside the Strömgen sphere is smaller than the gravitational potential energy at the I-front:

$$c_{\text{s},\infty}^2 < \frac{GM_{\text{bh}}}{R_{\text{s}}}. \quad (4)$$

### 3.2 RTI at the I-front

In the linear regime, the growth rate of the RTI at the interface between high-density ( $\rho_{\text{H}}$ ) and low-density ( $\rho_{\text{L}}$ ) media for a wave number  $k$  ( $= 2\pi/\lambda$ ) is  $\gamma = \sqrt{\mathcal{A}gk}$ , where the Atwood number is defined as  $\mathcal{A} \equiv (\rho_{\text{H}} - \rho_{\text{L}})/(\rho_{\text{H}} + \rho_{\text{L}})$ . Therefore the growth time-scale of the RTI  $\tau_{\text{RTI}}$  for linear perturbations with wavelength  $\lambda$  is

$$\tau_{\text{RTI}} = \gamma^{-1} = \sqrt{\frac{\rho_{\text{H}} + \rho_{\text{L}}}{\rho_{\text{H}} - \rho_{\text{L}}} \frac{\lambda}{2\pi g}} \sim \sqrt{\frac{\lambda}{2\pi g}}, \quad (5)$$

where  $g = GM_{\text{bh}}R_{\text{s}}^{-2}$  is the gravitational acceleration at the I-front and  $\mathcal{A}$  is close to unity if  $\rho_{\text{H}} \gg \rho_{\text{L}}$ . Assuming that the I-front is stationary (i.e. is not accelerating:  $L = \text{const}$ , and is not

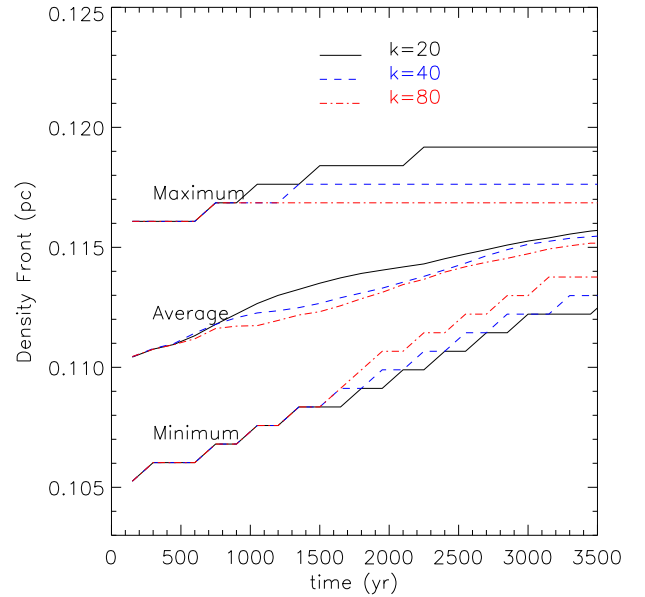


**Figure 3.** Suppression of RTI for different wavenumbers  $k = 20$  (solid), 40 (dashed) and 80 (dot-dashed). From top to bottom, each group of lines shows the maximum, average and the minimum loci of the I-fronts. Note that the average locations increase as a function of time (by about 5 per cent at  $t = 3500$  yr) due to the decreased density inside the H II region. The difference between the maximum and minimum locations decreases for each simulation as a function of time for all values of  $k$ . Simulations with bigger wavenumbers (i.e. shorter wavelengths) reach the spherical symmetry on slightly shorter time-scales with the initial perturbation suppressed by the radiation.

collapsing:  $R_{\text{s}} > r_{\text{B}}$ ), the RTI growth time-scale is

$$\tau_{\text{RTI}} \sim \sqrt{\frac{\lambda}{2\pi g}} = \sqrt{\frac{\lambda R_{\text{s}}^2}{2\pi GM_{\text{bh}}}} > \sqrt{\frac{\lambda R_{\text{s}}}{2\pi c_{\text{s},\infty}^2}}. \quad (6)$$

It is well known that recombination in the ionized gas is a stabilizing mechanism for I-fronts (Mizuta et al. 2005). This notion suggests that the RTI can be stabilized by recombination only if the RTI time-scale  $\tau_{\text{RTI}}$  is longer than the recombination time-scale  $\tau_{\text{rec}} \sim 1/n_{\text{H}}\alpha_{\text{rec}}$ . From this, we obtain that perturbations with wavelength  $\lambda > \lambda_{\text{crit}}$  are stabilized by recombination, where the critical wavelength is

$$\lambda_{\text{crit}} \equiv \frac{2\pi GM_{\text{bh}}\tau_{\text{rec}}^2}{R_{\text{s}}^2}. \quad (7)$$

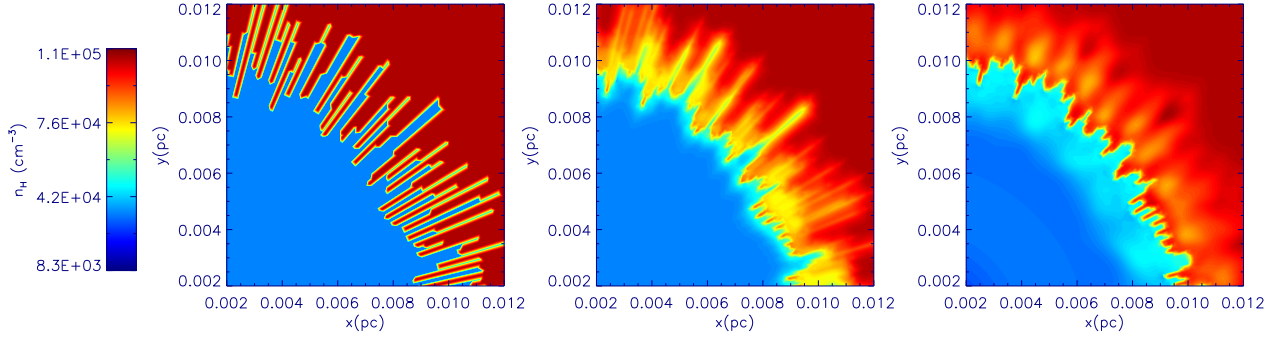


**Figure 4.** Simulation RANE3 for a BH mass  $M_{\text{bh}} = 100 M_{\odot}$ , gas density  $n_{\text{H},\infty} = 10^5 \text{ cm}^{-3}$  and the luminosity in Eddington unit  $l = 0.001$  with a random perturbation of I-front with a maximum of 20 per cent of the initial  $R_{\text{s}}$ . The smallest wavelength of  $\sim 0.0001 \text{ pc}$  set by the simulation resolution does not grow, but becomes suppressed by the photoionization and recombination effect.

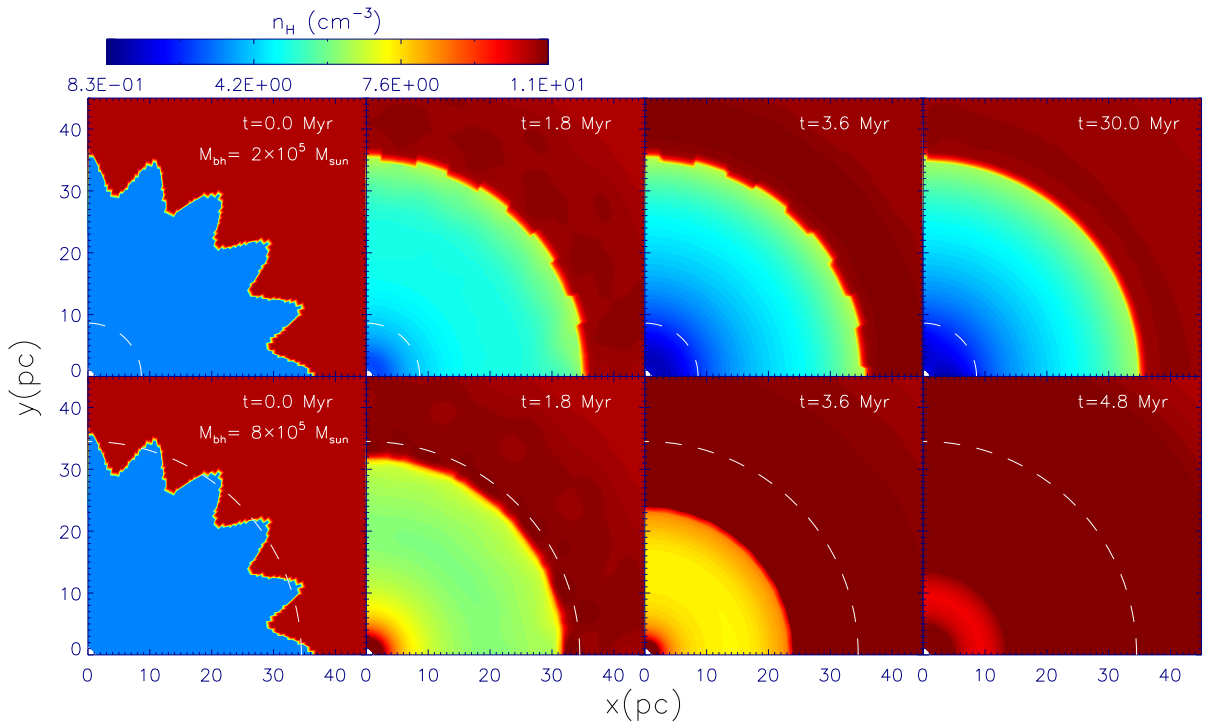


**Figure 5.** Top: evolution of the H II region for the run T4A with a BH mass  $M_{\text{bh}} = 2 \times 10^5 M_{\odot}$ , gas temperature  $T_{\infty} = 10^4 \text{ K}$  and density  $n_{\text{H},\infty} = 10 \text{ cm}^{-3}$ . Each panel displays the density profiles at  $t = 0.0, 1.8, 3.6$  and  $30.0 \text{ Myr}$ , respectively. Bottom: evolution of the run T4B with the same initial density, temperature, and BH luminosity as the top panels, but with a larger BH mass  $M_{\text{bh}} = 8 \times 10^5 M_{\odot}$ . Snapshots are taken at  $t = 0.0, 1.8, 3.6$  and  $4.8 \text{ Myr}$ , respectively. Dashed lines show the Bondi radius  $r_{\text{B}}$  for each BH mass  $M_{\text{bh}}$ . The Bondi radius for the run T4A is located within the H II region while the Bondi radius is comparable to the size of H II region for the run T4B. When the Bondi radius is comparable to or smaller than the size of the H II region, the entire H II region shrinks to the BH with the radiation trapped in the gas inflow.

If we define a critical angular scale of the perturbations  $\theta_{\text{crit}} \equiv \lambda_{\text{crit}}/2\pi R_{\text{s}}$ , using Equations (3) and (7) we find that scales  $\theta > \theta_{\text{crit}}$  are stable, where

$$\theta_{\text{crit}} \sim 5 \times 10^{-15} \frac{G}{\alpha_{\text{rec}} l} \sim \frac{2 \times 10^{-9}}{l}. \quad (8)$$

Thus,  $l$  needs to be very small ( $\sim 10^{-9}$ ) in order to observe the growth of RTI on scales comparable to the Strömgen radius. Given the limited resolution of finite grids of the current study, the development of the RTI can be observed only when  $l$  is extremely

low or the front is accelerating outwards, which makes the critical scale  $\theta_{\text{crit}}$  increase. This is indeed what has been observed in the simulations presented in Park & Ricotti (2011, 2012). If the effective gravitational acceleration at the I-front increases due to the front acceleration, larger wavelength can become unstable. The effective gravitational acceleration on the I-front increases when the I-front propagates against the gravity moving away from the BH. This occurs when the BH luminosity increases (see panels A and C in Fig. 1). See Whalen & Norman (2008) for details about the radiation hydrodynamic instabilities for propagating I-fronts.

Although we found that if  $l \leq 10^{-9}$  the I-front can be unstable to RTI, in this case we also expect that the I-front cannot be in equilibrium against the gravitational attraction of the BH because we are in the regime  $R_s < r_B$ . If we compare the RTI growth time-scale  $\tau_{\text{RTI}} \sim \tau_{\text{rec}}$  to the free-fall time-scale  $\tau_{\text{ff}} = R_s^{3/2} (2GM_{\text{bh}})^{-1/2}$  we find  $\tau_{\text{RTI}}/\tau_{\text{ff}} \propto l^{-1}$  implying that when  $l$  is small the RTI growth is slower than the time it takes for the I-front to collapse on to the BH.

### 3.3 Radiation-hydrodynamic Simulations

We run a set of 2D radiation-hydrodynamic simulations to examine the growth of the RTI at the I-front produced by radiation emitted by a BH. We use a parallel version of the non-relativistic hydrodynamic simulation code ZEUS-MP (Stone & Norman 1992; Hayes et al. 2006) with our 1D radiative transfer equation solver (Ricotti, Gnedin, & Shull 2001; Whalen & Norman 2006). We use an operator-split method switching between hydrodynamic and radiative transfer steps. For every time step, we use the smallest between the hydrodynamic and chemical time steps  $\Delta t = \min(\Delta t_{\text{hydro}}, \Delta t_{\text{chem}})$ . Our 1D radiative transfer subroutine calculates photoionization (and thus the chemistry of H I, H II, He I, He II, He III and  $e^-$ ), photoheating, and cooling. We assume that UV and X-ray photons are emitted from the BH centred at the origin of the spherical coordinate following a power-law spectrum ( $F_\nu \propto \nu^{-\alpha}$ ) with a spectral index  $\alpha = 1.5$  in the range of 13.6 eV–100 keV in 50 logarithmically spaced frequency bins. Radiative transfer equations are solved for each angular direction ( $\theta$ ) every time step. Radiation pressure on electron and neutral hydrogen (Park & Ricotti 2012) is not considered in the current work since simulations that included radiation pressure did not show significant differences from simulations that did not (Park & Ricotti 2011).

#### 3.3.1 Setting Up Initial Conditions

We adopt a constant luminosity,  $l$ , for a fixed BH mass,  $M_{\text{bh}}$ . The temperature ( $T_\infty = 10^4$  or  $10^3$  K) and the density  $n_{\text{H},\infty}$  of the surrounding gas are also constant in our initial conditions (ICs). From a given set of parameters, we calculate the Strömgen radius using Equation (3) and a lower density sphere with radius equal to the Strömgen radius is placed centred on the BH in the ICs set-up. The gas is initially assumed to be in pressure equilibrium. Thus, given the typical temperature  $T_{\text{in}} = 6 \times 10^4$  K in the lower density ionized sphere (Park & Ricotti 2012), the gas number density inside the Strömgen radius is  $n_{\text{H},\text{in}} = T_\infty/T_{\text{in}} n_{\text{H},\infty}$ . We perturb the spherical I-front by applying sinusoidal perturbations as  $R_s(\theta) = R_{s,0}(1 + \delta R_{s,0}/R_{s,0} \sin(k\theta))$ , where  $k$  is the wavenumber. The amplitude of the perturbations  $\delta R_{s,0}$  is a free parameter that we choose between 5, 10 and 20 per cent of  $R_{s,0}$ . For simulations K20E1–K20E5, we introduce random perturbations at the I-front for each radial direction resolved in the simulation. The Bondi radius is constant for a given temperature  $T_\infty$  and BH mass  $M_{\text{bh}}$ , while we vary the BH luminosity and thus the size of the H II region for a range of luminosities  $l$  between 0.1 and  $10^{-5}$  (see Table 1). In some simulations we fix the absolute BH luminosity  $L$  and vary the BH mass in order to explore the effect of changing the ratio  $r_B/R_s$ .

We perform 2D simulations in polar coordinate system ( $r, \theta$ ) with BHs centred at the origin assuming it is axisymmetric around  $\theta = 0$ . Evenly spaced 128–256 grids in the radial ( $r$ ) and polar angle ( $\theta$ ) directions are used to obtain higher resolution at the I-front.

In the radial direction, we set the box size of simulations twice the initial Strömgen radius  $R_{s,0}$  with flow-in boundary conditions and inner boundary between 0.02 and 0.2 of  $R_{s,0}$  with flow-out boundary conditions. The angular direction ( $\theta$ ) extends from 0 to  $0.5\pi$  and reflective boundary conditions are applied.

## 4 RESULTS

### 4.1 Suppression of RTI by Photoionization and Recombination

Simulations shown in panels (a)–(d) of Fig. 2 have the same IC (shown in the top panels): gas density ( $n_{\text{H},\infty} = 10^5 \text{ cm}^{-3}$ ), temperature ( $T_\infty = 10^4$  K) and perturbation wavelength ( $k = 20$ ). Each simulation differs for the presence/absence of an ionizing radiation field emitted by the BH and the initial ionization fraction inside the low-density bubble as summarized at the top of each panel (see Table 1).

Panels (a) and (b) in Fig. 2 show snapshots for simulations without radiation from the central BH (K20RTI and K20RTIrec in Table 1). The low-density region in the simulation K20RTI is neutral (H I) while in simulation K20RTIrec the gas is ionized (H II). Snapshot (a) shows an exponential growth of RTI when the simulation evolves to  $t = 45000$  yr. The high- and low-density media are initially in thermal equilibrium, but they start to mix with each other when the high-density gas accelerates on to the low-density region while the low-density fingers accelerate into the high-density region due to buoyancy. Panel (b) shows the snapshot taken at  $t = 7500$  yr for the simulation K20RTIrec which shows the effect of the recombinations in the initially ionized gas. Initial perturbations at the I-front are damped on a shorter time-scale compared to the typical RTI growth time-scale (panel a). As the simulation proceeds, the ionized gas recombines and the conditions become similar to the typical RTI condition as in panel (a).

However, when photoionization is turned on (panels c and d in Fig. 2), the simulations show that the growth of RTI fingers is suppressed at the I-front. The bottom panels in Fig. 2 show the simulations K20HI and K20HII with the radiation from the central BHs turned on, with the different initial ionization fraction of the low-density bubble (neutral gas in panel c and ionized gas in panel d). Both panels (c) and (d) show that the RTI fingers are suppressed. Dense fingers extended into the low-density region at the ICs are suppressed by the photoionization while the low-density fingers (in the dense medium) are also suppressed due to recombination. The I-front shown in panel (d) displays a smoother spherical shape compared to the one in panel (c). This is due to the effect of recombination since the I-front ionizes the inner region first and recombination dampen the perturbation before the I-front reaches the density discontinuity. The vector field of the bottom panels of Fig. 2 indicates that outflow inside the H II region also contributes in suppressing the inward motion of the dense RTI fingers as shown in panel (a). The outflow inside the H II region occurs due to the thermal pressure gradient as discussed in Park & Ricotti (2011, 2012) and serves as an important gas depletion mechanism inside the H II region. Thermal pressure gradient inside the H II region dominates the gravitational potential in the outer part of the Strömgen sphere causing the outflow seen in the bottom panels of Fig. 2. Note that simulations (c) and (d) do not reach a steady state due to the gas depletion inside the H II region; however, the growth of RTI is not observed.

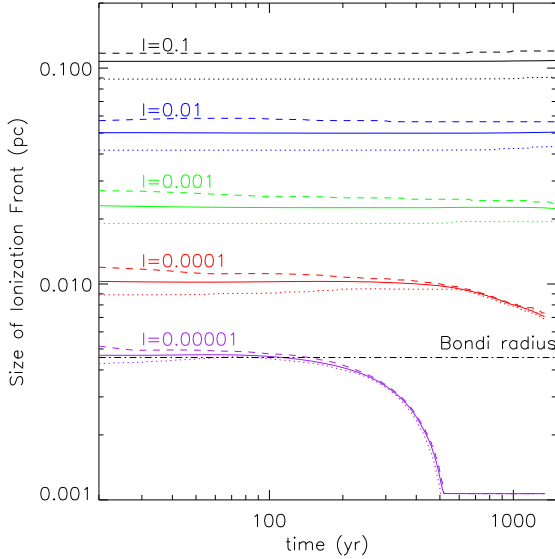


**Figure 6.** Stability of I-fronts as a function of the Eddington ratio  $l = L/L_{\text{Edd}}$  for a BH with mass  $M_{\text{bh}} = 100 M_{\odot}$  and gas density  $n_{\text{H},\infty} = 10^5 \text{ cm}^{-3}$ . When  $l > 0.001$ , the size of the H II region  $R_{\text{s}}$  is larger than the Bondi radius making the Strömgen sphere stable while the H II region shrinks to the BH when  $l \leq 10^{-5}$ , where the  $R_{\text{s}}$  becomes comparable to or smaller than the Bondi radius. This transition occurs because the sound crossing time-scale  $\tau_{\text{cross}}$  is shorter than the recombination time-scale  $\tau_{\text{rec}}$ . The amplitude of the initial perturbation decreases as a function of time not allowing the growth of RTI since the  $\tau_{\text{cross}}$  is shorter than the  $\tau_{\text{RT}}$ .

## 4.2 Suppression of the RTI as a function of wavenumber

In the linear regime of RTI growth, small-scale perturbations grow faster than large scales (see equation 5). Here, we examine how different wavelengths of RTI are affected by radiation.

Fig. 3 shows the evolution of the maximum, average and minimum location of I-fronts in simulations K20, K40 and K80 in Table 1 that differ for wavenumber of the initial perturbations:  $k = 20$  (solid lines), 40 (dashed lines) and 80 (dot-dashed lines). The average size of Strömgen sphere in all simulations increases as a function of time due to the decreasing density inside the H II region (the increase is about 5 per cent of the initial  $R_{\text{s}}$  at  $t = 3500$  yr). Relative locations of minimum/maximum density fronts converge asymptotically to the averages implying that the initial amplitude of the perturbations is damped. Note that the minimum radii of the I-fronts (RTI fingers) increase monotonically while the maximum loci do not increase much. The simulations also show that the amplitude of perturbations with larger wavenumbers (i.e. smaller wavelength) are suppressed on a shorter time-scales.

In Fig. 4, we show a simulation with random perturbations of the I-front in the ICs. The wavelength of the perturbations produced this way is limited by the angular resolution of the simulation. In this simulation, the maximum amplitude of the perturbation is 20 per cent of the size of H II region and the resolution in polar angle direction is  $R_{\text{s}}\Delta\theta = 0.01 \times 0.5\pi/128 = 0.0001 \text{ pc}$ . These simulations do not show any growth of the RTI even at the smallest scales permitted by the resolution. Qualitatively, the evolution is the same as in simulations with sinusoidal perturbations. With  $l = 0.1$  the critical angular scale from Equation (8) is  $\theta_{\text{crit}} \sim 10^{-11}$  radian implying that RTI on smallest scales that are not resolved in our simulations might not grow.

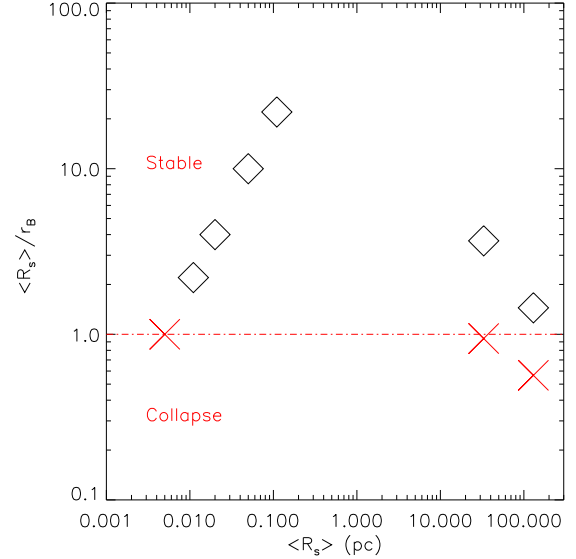


**Figure 7.** Stability of the I-front for various ratio between  $R_{\text{s}}$  and  $r_{\text{B}}$ . Diamonds indicates the simulations (RANE1–RANE4, T4A and T3A) showing stable I-fronts while crosses show the unstable simulations (RANE5, T4B and T3B) with collapsing Strömgen spheres. When  $R_{\text{s}}/r_{\text{B}} \leq 1$ , Strömgen sphere shrinks to the BH not being able to maintain the initial size of the Strömgen sphere.

## 4.3 Stability of I-fronts

In this section, we examine the stability of I-fronts varying the gravitational acceleration at the I-front. We vary the BH mass keeping the BH luminosity and  $R_{\text{s}}$  fixed. Hence, the luminosity in Eddington units  $l$  varies.

Fig. 5 shows the evolution of simulations with stable (upper panels) and unstable (lower panels) I-fronts. The stability of the I-front depends on the ratio  $R_{\text{s}}/r_{\text{B}}$  ( $R_{\text{s}}$  and  $r_{\text{B}}$  are shown as dashed lines). In this set of simulations (T4A/T4B and T3A/T3B), the BH luminosity is fixed and we set the BH mass  $M_{\text{bh}} = 2 \times 10^5 M_{\odot}$  in simulation T4A and  $M_{\text{bh}} = 8 \times 10^5 M_{\odot}$  in simulation T4B. The Bondi radius  $r_{\text{B}}$  is larger than  $R_{\text{s}}$  in the run T4A while  $r_{\text{B}} < R_{\text{s}}$  in run T4B. The simulation sets T3A and T3B are analogous, but the temperature of the ambient gas is  $T_{\infty} = 10^3 \text{ K}$  (instead of the fiducial value  $T_{\infty} = 10^4 \text{ K}$ ). The temperature of the gas inside the Strömgen sphere is  $T_{\text{in}} = 6 \times 10^4 \text{ K}$ ; thus, the density inside the Strömgen sphere is 60 times lower the ambient density (see Table 1).

Fig. 6 shows the stability of the I-front as a function of the luminosity  $l$ . When  $l$  is larger than  $10^{-3}$ , the I-fronts are stable since the  $R_{\text{s}}$  is larger than the Bondi radius, while the I-fronts collapse towards the BH for  $l \leq 10^{-5}$  when  $R_{\text{s}} \sim r_{\text{B}}$ . Note that the initial perturbations are suppressed even when the I-front collapses.

Fig. 7 shows the stability of the I-fronts for all the simulations listed in Table 1 showing that the ratio  $R_{\text{s}}/r_{\text{B}}$  determines the stability of the I-front. Simulations RANE5, T4B and T3B in Table 1 have  $R_{\text{s}}/r_{\text{B}} \leq 1$  and indeed their I-fronts collapse on to the BHs while the I-fronts are stable in all the other simulations that have  $R_{\text{s}}/r_{\text{B}} > 1$ . In all simulations the initial perturbations at the I-front are suppressed creating a spherically symmetric H II region, however, when  $R_{\text{s}}/r_{\text{B}} \leq 1$  the ionized region collapses on to the central BH with the radiation from the BH trapped by the inflowing gas.

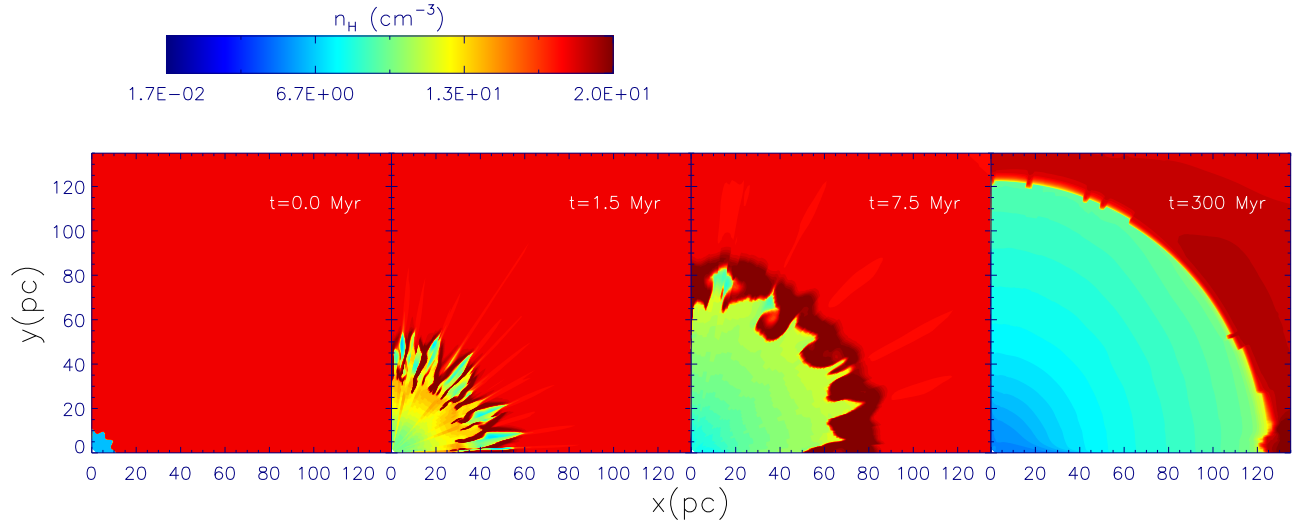


**Figure 8.** Snapshots for a simulation T3ABURST with a luminosity burst. Most of the parameters at the IC is identical to the simulation T3A which shows the suppressed RTI, but the initial size of  $R_s$  for this run is 10 times smaller. Since the BH luminosity is large enough to create a 10 times larger H II region, the H II bubble expands until it finds an equilibrium (at  $R_s \sim 130$  pc). Due to the expansion of the H II region, RTI is observed at the initial phase of the simulation, however RTI becomes suppressed as the I-front reaches the equilibrium radius which is set by the BH luminosity.

#### 4.4 RTI with a burst of luminosity

Finally, we simulate the case when the I-front propagates outward against the gravity, increasing the value of the effective acceleration in the frame of reference of the I-front. Fig. 8 shows the evolution of the H II region which expands following a luminosity burst. The initial luminosity is the same as in simulation T3A corresponding to a Strömgen sphere with  $R_s = 130$  pc. But here we decrease the size of the low-density region by a factor of 10 in the ICs. The I-front expands since the equilibrium size of H II region for the given BH luminosity is larger than the radius of the contact discontinuity in the ICs. The development of the RTI is observed at the beginning of the simulation during the outward propagation of the I-front. However, the RTI is suppressed as the I-front reaches the Strömgen radius set by the BH luminosity. We thus conclude that stationary I-fronts produced by BHs accreting from a neutral medium are stable to the development of RTI. Only an accelerating I-front produced by an accretion and luminosity burst develops RTI.

## 5 SUMMARY AND DISCUSSION

In this paper, we examine the growth and suppression of RTI at the I-front around BHs. This is a follow-up study on our previous works on radiation-regulated accretion on to BHs (Park & Ricotti 2011, 2012). We use numerical techniques that couple radiation to hydrodynamics and focus on the condition of RTI development at the I-front. In general, our radiation-hydrodynamic simulations do not show growth of RTI in the presence of the ionizing radiation from BHs, which agrees with the perturbation analysis of the linear growth of RTI (Ricotti 2013). The following is a summary of the main findings:

- For non-accelerating I-fronts, the RTI is stabilized on all scales resolved in our simulations.
- Our calculations show that the wavelength of the unstable modes is inversely proportional to the luminosity  $l$  in Eddington units, but when  $l$  is small the I-front collapses on to the BH for

because  $R_s < r_B$ , preventing the development of the RTI in all realistic cases.

- Accelerating I-fronts, produced during a luminosity burst, become unstable to RTI but are quickly stabilized by the radiation when the burst ends.

The findings in this study are relevant for understanding the role of radiation in suppressing the RTI at the I-front around luminous gravitating sources such as BHs or proto-stars. For quasi-spherically symmetric systems, the RTI is not an efficient mechanism for delivering gas from large scales to the central gravitating source. For systems with high angular momentum, the spherical symmetry assumed in this study is not realistic and the RTI might play an important role in particular directions where the radiation flux is reduced due to enhanced gas column density (e.g., Krumholz et al. 2009). Due to the limited degrees of freedom in our 2D simulations, more realistic 3D simulations might display slightly different results. Nonetheless, the qualitative description of the role of photoionization on RTI presented in this work should still be valid.

## ACKNOWLEDGEMENTS

This research is supported by the Urania E. Stott Fellowship of The Pittsburgh Foundation. MR’s research is supported by NASA grant NNX10AH10G, NSF CMMI1125285 and ILP LABEX (under reference ANR-10-LABX-63) supported by French state funds managed by the ANR within the Investissements d’Avenir programme under reference ANR-11-IDEX-0004-02. TDM acknowledges the National Science Foundation, NSF Petapps, OCI-0749212 and NSF AST-1009781 for support. KP thanks James Drake for the motivation of this paper, and the anonymous referee for useful comments. The numerical simulations in this paper were performed using the computer cluster (“yorp”) of the Center for Theory and Computation, the Department of Astronomy at the University of Maryland at College Park.



## REFERENCES

- Bondi H., Hoyle F., 1944, MNRAS, 104, 273  
Bondi H., 1952, MNRAS, 112, 195  
Chandrasekhar S., 1961, Hydrodynamic and Hydromagnetic Stability. Dover Press, New York  
Hayes J. C., Norman M. L., Fiedler R. A., Bordner J. O., Li P. S., Clark S. E., ud-Doula A., Mac Low M.-M., 2006, ApJS, 165, 188  
Jacquet E., Krumholz M. R., 2011, ApJ, 730, 116  
Jiang Y.-F., Davis S. W., Stone J. M., 2013, ApJ, 763, 102  
Kahn F. D., 1958, Rev. Mod. Phys., 30, 1058  
Krolik J. H., 1977, Phys. Fluids., 20, 364  
Krumholz M. R., Klein R. I., McKee C. F., Offner S. S. R., Cunningham A. J., 2009, Science, 323, 754  
Krumholz M. R., Matzner C. D., 2009, ApJ, 703, 1352  
Kuiper R., Klahr H., Beuther H., Henning T., 2012, A&A, 537, A122  
Li Y., 2011, preprint (arXiv:1109.3442)  
Milosavljević M., Couch S. M., Bromm V., 2009, ApJ, 696, L146  
Mizuta A., Kane J. O., Pound M. W., Remington B. A., Ryutov D. D., Takabe H., 2005, ApJ, 621, 803  
Park K., Ricotti M., 2011, ApJ, 739, 2  
Park K., Ricotti M., 2012, ApJ, 747, 9  
Park K., Ricotti M., 2013, ApJ, 767, 163  
Ricotti M., Gnedin N. Y., Shull J. M., 2001, ApJ, 560, 580  
Ricotti M., 2013, MNRAS, arXiv(1310.1459)  
Stone J. M., Norman M. L., 1992, ApJS, 80, 753  
Taylor G., 1950, Proc. R. Soc., 201, 192  
Whalen D., Norman M. L., 2006, ApJS, 162, 281  
Whalen D. J., Norman M. L., 2008, ApJ, 672, 287